Click Here for Full Article

Imaging hydraulic fractures in a geothermal reservoir

Bruce R. Julian,[1,2] Gillian R. Foulger,[3] Francis C. Monastero,[4] and Steven Bjornstad[5]

[1]   An injection experiment at the Coso geothermal field in eastern California in March 2005 caused a swarm of micro-earthquakes that was recorded by a local network of three-component digital seismometers. High-resolution relative hypocenter locations propagated upward and northward on a 700 × 600 m plane striking N 20°E and dipping 75° to the WNW. This plane is a pre-existing fault, whose surface projection coincides with an active scarp. The earthquakes have similar non-double-couple mechanisms that involve volume increases, and the fault plane bisects their dilatational fields, implying a process dominated by tensile failure. The source types require the additional involvement of subsidiary shear faulting, however. Events before and after the swarm have variable orientations and volume changes of both signs. Similar tensile-shear failure is observed in some natural microearthquake swarms, for example at Long Valley caldera, California. Its occurrence under low fluid pressure may imply a heterogeneous stress field or the induction of thermal stresses by introduction of cold fluid. **Citation:** Julian, B. R., G. R. Foulger, F. C. Monastero, and S. Bjornstad (2010), Imaging hydraulic fractures in a geothermal reservoir, *Geophys. Res. Lett.*, *37*, L07305, doi:10.1029/2009GL040933.

1. Introduction

[2]   The Coso geothermal area lies in the southwestern corner of the Basin and Range province in eastern California, at a right (releasing) step-over in the southern Owens Valley fault zone, which experiences 6.5 ± 0.7 mm/year of dextral shear [*Monastero et al.*, 2005]. The geothermal area has been exploited since the 1980s to produce electric power.

[3]   In February and March of 2005 an "Enhanced Geothermal Systems" (EGS) experiment was conducted in injector well 34-9RD2 on the east flank of the reservoir to increase permeability and enhance production in a cluster of wells about 1 km to the south. The well was re-worked in order to introduce fluids into a target formation near its bottom. The existing slotted liner was removed, open fractures and washout regions were cemented and repaired, an un-slotted liner was inserted, and the well was then deepened. Major circulation-loss zones were encountered at a depth of 2654 m, and a total loss of drilling mud occurred at a depth of about 2672 m while injecting water at rates up to 20 l/s.

[4]   This injection caused a vigorous swarm of earthquakes, which we analyzed using data from a local 36-station seismic network. We determined high-resolution relative hypocenter locations and complete (symmetric moment-tensor) source mechanisms for many of the earthquakes. Relative hypocenter locations provide information about the geometry of the failure zone that complements seismic moment tensors and reduces inherent ambiguities in their physical interpretation. Surface geological observations subsequently verified the inferred fault geometry. The results of this experiment demonstrate that seismological techniques can provide information of high quality about hydraulic fractures that are of potential value for operational decision-making.

2. Data and Methods

[5]   The Geothermal Program Office of the U.S. Navy monitors seismicity at Coso, operating 22 digital three-component short-period seismometers at depths of about 100 m in custom-drilled boreholes. To enhance this network near the planned EGS experiment, we installed 16 additional digital three-component seismic stations on the surface. We choose optimal locations for these stations by computing theoretical focal-sphere positions of candidate sites by numerically tracing rays [*Arnott and Foulger*, 1994; *Julian et al.*, 1996; *Miller et al.*, 1998] through a three-dimensional crustal wave-speed model [*Wu and Lees*, 1999] obtained from local earthquake tomography. The injection induced a swarm of about 70 recorded earthquakes, almost all within the first hour, between 03:00 and 04:00 GMT March 3rd (Figure 1). Most of the earthquakes occurred in the first two minutes. A total of 44 earthquakes with M from 0.3 to 2.6 were detected and located by the U.S. Navy permanent network.

[6]   We measured the arrivals from both networks by hand and located the earthquakes using *hypocc*, an optimized and corrected version of the method of *Waldhauser and Ellsworth* [2000] to simultaneously invert the inter-event arrival-time differences for many events to obtain accurate relative hypocenter locations. *hypocc* speeds computations by using dynamic storage allocation and efficient algorithms such as depth-first graph searching and data structures such as hash tables [*Knuth*, 1973, section 6.4] and k-dimensional binary search trees [*Knuth*, 1973, section 6.5] for analyzing the complex relationships within large data sets.

[7]   We computed full (symmetric) moment tensors by using linear-programming methods to invert observed *P*-, *SH*-and *SV*-phase polarities and *P:SH*, *P:SV*, and *SH:SV* amplitude ratios measured from low-pass filtered seismograms (corner frequency 5 Hz, 3-pole Butterworth response), as described by *Julian and Foulger* [1996]. Earthquakes

[1]U.S. Geological Survey, Menlo Park, California, USA.
[2]Now at Foulger Consulting, Palo Alto, California, USA.
[3]Department of Earth Sciences, Science Laboratories, University of Durham, Durham, UK.
[4]Magma Energy U.S. Corp., Reno, Nevada, USA.
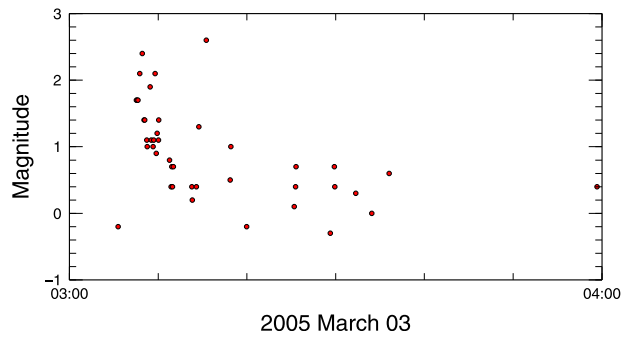[5]Geothermal Program Office, China Lake, California, USA.

Figure 1. Magnitudes of earthquakes within 1.1 km of the bottom of well 34-9RD2 for the period 03:00–04:00 March 3rd, 2005.

associated with geothermal areas and hydrofracturing typically involve significant volume changes, which require moment tensors for their description [*Foulger*, 1988; *Foulger and Long*, 1984; *Foulger and Julian*, 1993, 2004; *Foulger et al.*, 1989; *Julian and Foulger*, 2004; *Julian et al.*, 1997, 2004; *Miller et al.*, 1998; *Ross et al.*, 1996, 1999].

[8] The extra degrees of freedom afforded by the moment-tensor representation make it important to assess the uniqueness of derived mechanisms. This is a subject of great current interest and the state of the art is changing rapidly. Preliminary confidence regions based on the variation of the L1 norm of the data residuals [*Julian and Foulger*, 2008] indicate that the variations found in this study are well resolved, as do also the systematic variations of mechanisms with time discussed below.

3. Results

[9] The U.S. Navy catalog earthquake hypocenter locations, which are computed using a one-dimensional layered crustal model (K. Richards-Dinger, personal communication, 2004), form a diffuse cluster distributed throughout most of the area of production wells south of the injector (Figure 2). The accuracy of such hypocenter locations is difficult to estimate, because the major source of error is uncertainty about crustal structure, not measurement error. As is typical for earthquakes located individually in this manner, the locations do not resolve structures on the scale of a few tens of meters, as is necessary if the results are to be of use for scientific understanding and operational decision-making. The relative relocations, in contrast, clearly resolve a plane with a strike of N 20°E dipping 75° to the WNW with dimensions of about 700–600 m. This activated structure lies about 500 m southeast of the injector.

[10] We obtained high-quality moment tensors for 14 of the largest earthquakes (Figure 3). For comparison, we also computed moment tensors for seven pre-injection earthquakes and 17 post-injection earthquakes in March 2005. The mechanisms of small geothermal earthquakes in tectonic environments typically lie near the line connecting the
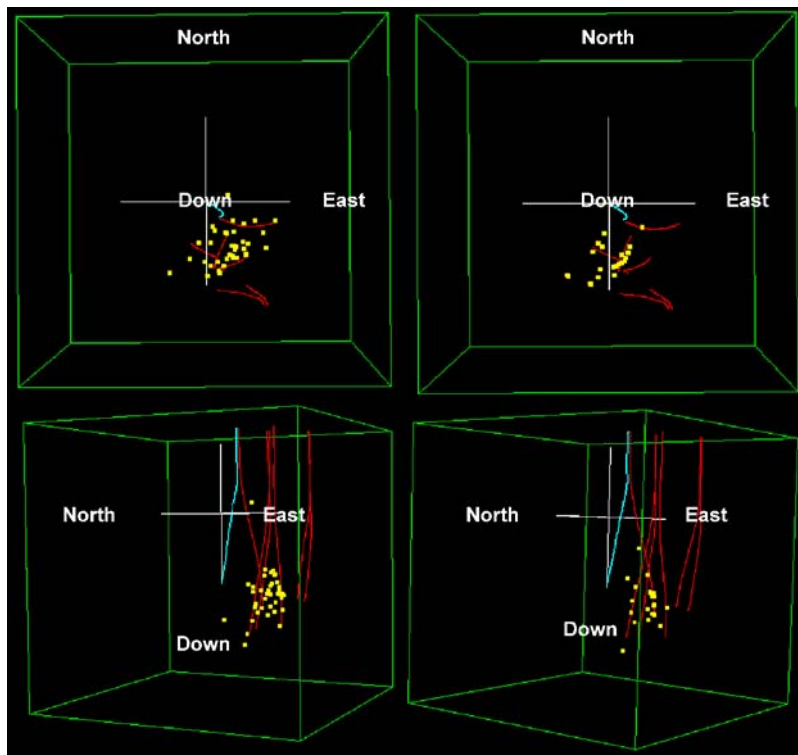

Figure 2. Perspective views showing locations of earthquakes: (top) downward-directed views and (bottom) sub-horizontal views with lines of sight along the plane defined by the hypocenters. Blue line: well 34-9RD2; red lines: wells 34A-9, 38A-9, 38C-9, 38B-9, 38-9, 51-16 and 51A-16. (left) U.S. Navy catalog locations and (right) relative relocations calculated using *hypocc* [*Julian and Foulger*, 2008]. The green box is 4 × 4 × 4 km. The white lines indicate coordinate directions, and are centered at sea level directly above the bottom of well 34-9RD2.
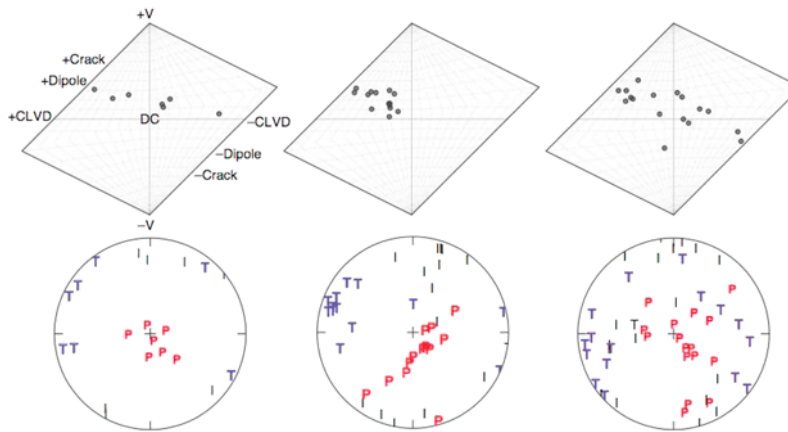
Figure 3. (top) Source-type plots [*Hudson et al.*, 1989] of the mechanisms of (left) pre-, (middle) co- and (right) post-injection-swarm earthquakes. (bottom) Source-orientation plots showing the principal-moment directions for the same earthquake sets. Upper focal hemispheres are shown in equal-area projection.

+dipole and −dipole points on the source-type plot of *Hudson et al.* [1989] and the post-injection earthquakes conform to this pattern. Dipole source types could be interpreted as opening or closing tensile cracks, with volume changes partly compensated by fluid inflow. Sources with implosive components are absent from the pre-injection earthquakes, but this absence probably is an artifact of the small size of the pre-injection data set; implosive micro-earthquakes did occur during the previous month. Implosive mechanisms are entirely lacking from the co-injection swarm earthquakes, probably because of either increased fluid pressure or tensile stresses caused by induced thermal contraction.

[11] The *T* axes of most of the earthquakes have approximately horizontal, east-west orientations. In contrast, the *P* axes show significant variation. For the co-injection swarm earthquakes, the *T* axes are tightly clustered to the WNW and the *P* axes occupy a narrow zone extending from nearly vertical to horizontal and trending to the southwest.

This distribution differs markedly from that either before or after the injection.

[12] The co-injection swarm earthquakes have similar source mechanisms (Figure 4). All the earthquakes studied have mechanisms consistent with combined normal and strike-slip motion — the *P* polarity plots resemble those of normal-faulting earthquakes, but with reduced dilatational fields with partially explosive mechanisms, i.e., they correspond to opening cavities.

4. Discussion

[13] The interpretation of moment tensors in terms of physical source processes is not unique [*Julian et al.*, 1998]. The mechanisms shown in Figure 4 could represent shear slip on faults dipping at various angles to either the WNW or the ESE, combined with a process such as tensile cracking that involves a volume increase. Reducing this ambiguity requires additional independent information [*Foulger et al.*, 2004].
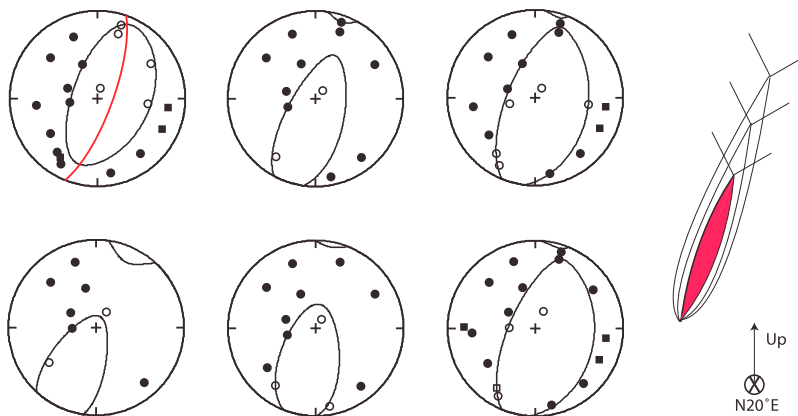

Figure 4. Moment tensors for 6 typical earthquakes of the 14 studied from the injection swarm, displayed as *P*-wave polarity plots. Black lines: nodal curves. Red line: the fault delineated by the relative relocations (Figure 2). Open/solid circles: dilatational/compressional arrivals on the upper focal hemisphere; open/solid squares: dilatational/compressional arrivals on the lower focal hemisphere; pluses: the center of the focal hemisphere. At right is a schematic illustration of shear wing faults associated with a propagating tensile crack. The view is along the plane of the crack, which in this case strikes to the NNE and dips steeply to the WNW.
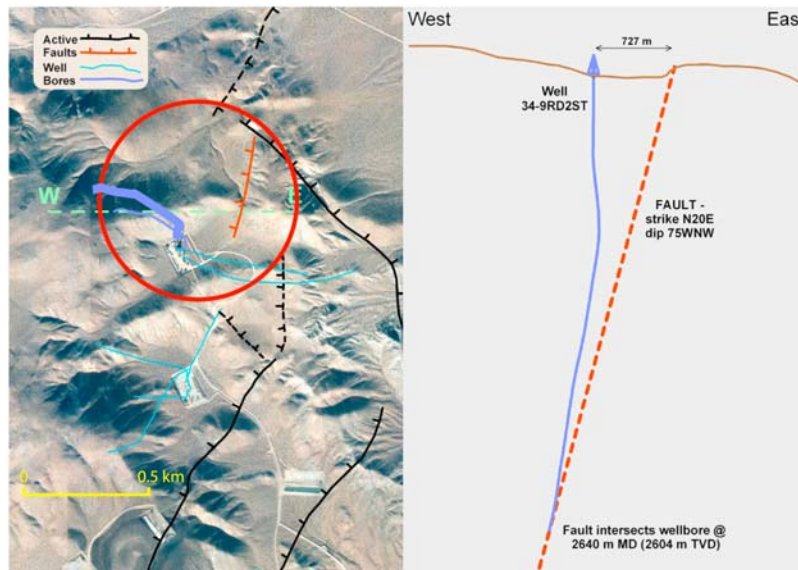
Figure 5. Geological confirmation of the fault delineated by microearthquake hypocenters. (left) Map showing the surface projection of well 34-9RD2 (violet), other wells (blue), the surface traces of Quaternary faults (black), and the fault identified with the earthquake swarm (red). (right) West-east vertical cross-section showing well 34-9RD2 and interpolation between the surface Quaternary fault scarp and the fault zone imaged in the televiewer log.

[14] On the focal-sphere plot at the top left of Figure 4, the fault plane defined by the relative hypocenter locations (Figure 2) is superimposed on the theoretical *P*-phase nodal curves for the moment tensor. This line, which indicates the main structure activated, bisects the dilatational field. If the structure were a shear fault, the line would lie close to a nodal curve of the focal mechanism, but this is not the case to a high degree of confidence. A fault bisecting the dilatational field is, however, expected for a hydraulically driven tensile crack [*Julian et al.*, 1998]. Similar observations have been reported previously, *e.g.*, for naturally occurring swarm microearthquakes in the south moat of Long Valley caldera, California [*Foulger et al.*, 2004].

[15] The injection probably stimulated a pre-existing fault to fail. The largest earthquake of the swarm was of M 2.6, which corresponds to failure of a plane with dimensions of no more than a few tens of metres. This fact suggests that the ~600-m-long activated fault existed prior to the injection and was stimulated by the injection to fail in tensile mode. Each individual earthquake probably represents opening of a portion of the fault accompanied by subsidiary motion on shear wing faults (Figure 4, right). Seismic activity propagated northeast and upward during the swarm.

[16] Surface geological observations confirm the existence of the inferred fault (Figure 5). The scarp of a Quaternary fault, striking slightly east of north and dipping steeply to the WNW occurs in surface sediments northeast of the well at the position obtained by extrapolating the plane of microearthquake hypocenters to the surface. In addition, a televiewer borehole log of well 34-9RD2 provides evidence of a fault intersecting the well near its bottom.

[17] Hydraulic fracturing stress tests conducted in nearby boreholes confirm that the faulting regime of the Coso East Flank is transitional from normal to strike-slip. The azimuth of the smallest horizontal principal stress throughout the area is $108° ± 24°$, a range consistent with the orientation of the activated fault. The relative magnitudes of ambient stresses are such that normal faulting can be induced by increases in reservoir pressure of >3.5 MPa, and strike-slip faulting by smaller pressure increases. The magnitude of the compressive stresses inferred from the hydrofracture tests are inconsistent with our observation of tensile failure, however, as the hydraulic pressure of 2672 m of drilling mud is much smaller (the wellhead pressure was zero). This inconsistency is presently unresolved. It might point to large local heterogeneities in stress, to the importance of thermal stresses caused by the sudden introduction of cold drilling mud into the fault zone, or some other currently unidentified process.

5. Conclusions

[18] An injection of drilling mud at a depth of 2672 m in well 34-9RD2 at the Coso geothermal area induced a vigorous earthquake swarm in March of 2005 that lasted approximately an hour, with most of the seismic energy release occurring in the first two minutes. A detailed picture of fracture formation was obtained from a combination of relative hypocenter locations and moment tensors.

[19] The swarm activated about 700–600 m of a pre-existing fault. This fault opened in tensile mode, with each small earthquake corresponding to tensile opening of the main structure, along with subsidiary shear on wing faults oblique to the main fault. The existence of the structure deduced from seismic evidence is confirmed by surface geological observations and by data from a borehole televiewer log. Hydraulic fracturing stress tests indicate omnicompressional stresses in boreholes in this part of the geothermal area, so it is not clear how tensile failure can occur as a result of the injection of drilling mud under only hydrostatic pressure. This is a problem associated with explaining the volumetric components commonly found in the mechanisms of small earthquakes in fluid reservoirs. It

may be an indication that local stresses in such environments are highly inhomogeneous.

[20] This case history is an important landmark in the recent development of seismological techniques in support of Enhanced Geothermal Systems hydrofracturing experiments. It demonstrates that seismological instruments, field operations, data processing tools and interpretive experience have matured to the extent that they can deliver information of utility to operational decision-making.

References

Arnott, S. K., and G. R. Foulger (1994), The Krafla spreading segment, Iceland: 1. Three-dimensional crustal structure and the spatial and temporal distribution of local earthquakes, *J. Geophys. Res.*, *99*, 23,801–23,825, doi:10.1029/94JB01465.

Foulger, G. R. (1988), Hengill triple junction, SW Iceland: 2. Anomalous earthquake focal mechanisms and implications for process within the geothermal reservoir and at accretionary plate boundaries, *J. Geophys. Res.*, *93*, 13,507–13,523, doi:10.1029/JB093iB11p13507.

Foulger, G. R., and B. R. Julian (1993), Non-double-couple earthquakes at the Hengill-Grensdalur volcanic complex, Iceland: Are they artifacts of crustal heterogeneity?, *Bull. Seismol. Soc. Am.*, *83*(1), 38–52.

Foulger, G. R., and B. R. Julian (2004), A powerful tool: Use of time-dependent MEQ tomography for monitoring producing geothermal reservoirs, *Geotherm. Res. Counc. Bull.*, *33*, 120–126.

Foulger, G. R., and R. E. Long (1984), Anomalous focal mechanisms: Tensile crack formation on an accreting plate boundary, *Nature*, *310* (5972), 43–45, doi:10.1038/310043a0.

Foulger, G. R., R. E. Long, P. Einarsson, and A. Björnsson (1989), Implosive earthquakes at the active accretionary plate boundary in northern Iceland, *Nature*, *337*(6208), 640–642, doi:10.1038/337640a0.

Foulger, G. R., B. R. Julian, D. P. Hill, A. M. Pitt, P. E. Malin, and E. Shalev (2004), Non-double-couple microearthquakes at Long Valley caldera, California, provide evidence for hydraulic fracturing, *J. Volcanol. Geotherm. Res.*, *132*(1), 45–71, doi:10.1016/S0377-0273(03)00420-7.

Hudson, J. A., R. G. Pearce, and R. M. Rogers (1989), Source type plot for inversion of the moment tensor, *J. Geophys. Res.*, *94*, 765–774, doi:10.1029/JB094iB01p00765.

Julian, B. R., and G. R. Foulger (1996), Earthquake mechanisms from linear-programming inversion of seismic-wave amplitude ratios, *Bull. Seismol. Soc. Am.*, *86*(4), 972–980.

Julian, B. R., and G. R. Foulger (2004), Microearthquake focal mechanisms: A tool for monitoring geothermal systems, *Geotherm. Res. Counc. Bull.*, *33*, 166–171.

Julian, B. R., and G. R. Foulger (2008), Moment-tensor confidence regions from seismic-wave amplitude ratios, paper presented at 31st General Assembly, Eur. Seismol. Comm., Hersonissos, Greece.

Julian, B. R., A. Ross, G. R. Foulger, and J. R. Evans (1996), Three-dimensional seismic image of a geothermal reservoir: The Geysers, California, *Geophys. Res. Lett.*, *23*(6), 685–688, doi:10.1029/95GL03321.

Julian, B. R., A. D. Miller, and G. R. Foulger (1997), Non-double-couple earthquake mechanisms at the Hengill-Grensdalur volcanic complex, southwest Iceland, *Geophys. Res. Lett.*, *24*(7), 743–746, doi:10.1029/97GL00499.

Julian, B. R., A. D. Miller, and G. R. Foulger (1998), Non-double-couple earthquakes: 1. Theory, *Rev. Geophys.*, *36*(4), 525–549, doi:10.1029/98RG00716.

Julian, B. R., G. R. Foulger, and K. Richards-Dinger (2004), The Coso geothermal area: A laboratory for advanced MEQ studies for geothermal monitoring, paper presented at Annual Meeting, Geotherm. Resour. Counc., Indian Springs, Calif.

Knuth, D. E. (1973), *Sorting and Searching*, 723 pp., Addison-Wesley, Reading, Mass.

Miller, A. D., B. R. Julian, and G. R. Foulger (1998), Three-dimensional seismic structure and moment tensors of non-double-couple earthquakes at the Hengill-Grensdalur volcanic complex, Iceland, *Geophys. J. Int.*, *133*(2), 309–325, doi:10.1046/j.1365-246X.1998.00492.x.

Monastero, F. C., A. M. Katzenstein, J. S. Miller, J. R. Unruh, M. C. Adams, and K. Richards-Dinger (2005), The Coso geothermal field: A nascent metamorphic core complex, *Geol. Soc. Am. Bull.*, *117*(11–12), 1534–1553, doi:10.1130/B25600.1.

Ross, A., G. R. Foulger, and B. R. Julian (1996), Non-double-couple earthquake mechanisms at the Geysers geothermal area, California, *Geophys. Res. Lett.*, *23*(8), 877–880, doi:10.1029/96GL00590.

Ross, A., G. R. Foulger, and B. R. Julian (1999), Source processes of industrially-induced earthquakes at the Geysers geothermal area, California, *Geophysics*, *64*(6), 1877–1889, doi:10.1190/1.1444694.

Waldhauser, F., and W. L. Ellsworth (2000), A double-difference earthquake location algorithm: Method and application to the northern Hayward fault, California, *Bull. Seismol. Soc. Am.*, *90*(6), 1353–1368, doi:10.1785/0120000006.

Wu, H., and J. Lees (1999), Three-dimensional *P* and *S* wave velocity structures of the Coso geothermal area, California, from microseismic travel time data, *J. Geophys. Res.*, *104*, 13,217–13,233, doi:10.1029/1998JB900101.

S. Bjornstad, Geothermal Program Office, 429 East Bowen Rd., Stop 4011, China Lake, CA 93555-6108, USA.

G. R. Foulger, Department of Earth Sciences, Science Laboratories, University of Durham, South Road, Durham DH1 3LE, UK.

B. R. Julian, Foulger Consulting, 1025 Paradise Way, Palo Alto, CA 94306, USA. (bruce@foulgerconsulting.com)

F. C. Monastero, Magma Energy U.S. Corp., 9740 S. McCarran Blvd., Ste. 103, Reno, NV 89523-9204, USA.